Solid Freeform Fabrication 2022: Proceedings of the 33rd Annual International Solid Freeform Fabrication Symposium – An Additive Manufacturing Conference
Reviewed Paper

In-situ Integration of Weldable Strain Gauges in Components Manufactured by Laser-based Powder Bed Fusion

Maximilian Binder[1,2*], Andreas Machnik[3], Maximilian Bosch[1], Katharina Kreitz[3], Georg Schlick[1], Christian Seidel[1,4]

[1]Fraunhofer Institute for Casting, Composite and Processing Technology IGCV, Am Technologiezentrum 10, 86159 Augsburg, Germany
[2]Technical University of Munich, Institute for Machine Tools and Industrial Management, Boltzmannstr. 15, 85748 Garching, Germany
[3]Vectoflow GmbH, Friedrichshafener Str. 1, 82205 Gilching, Germany
[4]Munich University of Applied Science, Department of Applied Science and Mechatronics, Lothstr. 34, 80335 Munich, Germany
*Corresponding author: maximilian.binder@igcv.fraunhofer.de

Abstract

The integration of sensors in components made by PBF-LB/M facilitates promising new possibilities for component monitoring. It enables the collection of relevant measurement data at previously inaccessible component regions, which are needed for the determination of maintenance strategies. Therefore, the following research deals with the development of a concept, with which weldable strain gauges (WSG) can be weld-on by the laser-scanner-system of a PBF-LB/M system to the manufactured component. The examinations show that the arrangement of so-called weld seams has a decisive influence on a correct metal carrier connection of the WSG. It can be deduced from the study that WSGs can be integrated within components manufactured by PBF-LB/M and completely welded to it with the laser-scanning-system. Following measurement validations demonstrate that the WSG provides complete and correct measurement data and can therefore be considered as successfully connected to the component.

Keywords: Laser-Based Powder Bed Fusion, Metal Additive Manufacturing, Strain Gauges, Smart Parts, Inconel

Introduction

Additive Manufacturing (AM) in general describes technologies to produce components by successive addition of material and are usable for a wide range of applications in industry. Present statistics indicate a vigorously growing of AM industry over the next several years (Compound Annual Growth Rate of 23.3 %), because of its potential to generate a variety of economic benefits, like manufacturing of individual products and efficiency improvements in production [1,2]. The expansion of the current state of the art is therefore of great technical and economic interest.

Recent studies investigating developments and white spots in additive manufacturing identified the embedding of sensors in AM components as one of the most important trends with a high need for research [3–5]. The benefit of the layer-by-layer process is the possibility of sensor integration at any time during the process and at any area within the manufactured part [6–9]. Through the surrounding component, an integrated sensor can be protected from external environmental influences, is not visible from the outside and does not influence its geometrical shape. In addition

structural weakness of the part through sensor integration can be minimized and therefore a high functional density be realized. These advantages allow the acquisition of relevant measurement data at previously inaccessible component sections. This approach can potentially improve the implementation of predictive maintenance methods and capture more accurate process data that enables advanced process control for processing machines in the chemical industry, for example.

The integration of sensors during the metalworking laser-based powder bed fusion (PBF-LB/M) [10] process requires an extension of the existing manufacturing process. This involves a process interruption at any cross section layer of the component to be manufactured, while at the same time it must correspond to the top of a cavity manufactured within the component. In addition, the loose metal powder inside must be removed, the sensor integrated, and the manufacturing process continued. Sensor integration during the PBF-LB/M process involves numerous challenges, which must first be considered and overcome. On the one hand, the sensor to be integrated must be able to withstand the high temperature gradients during the manufacturing process and must not be damaged by them. On the other hand, a sufficient connection to the carrier component must be ensured so that the sensor supplies correct and usable measurement data. Care must also be taken to ensure that the internal cavity in which the sensor is integrated does not have any negative effects on neither the component strength nor the accuracy of the sensor.

The strain gauges are considered promising for numerous measurement tasks and are thus among the most widely used sensors for component monitoring. Strain gauges are sensors for measuring stretching and compressing deformations. They are also suitable for stress analysis. For this, the mechanical stresses prevailing in an object are determined from the measured deformations by applying the corresponding material laws. Depending on the strain gage design and the resulting measurement requirements, the application can be carried out in various ways. In addition to conventional adhesive bonding, which is prevalent in the PBF-LB/M process due to the metal powder particles present and which can severely impair this process, it is also possible to weld the strain gauges to the component surface using an appropriate metal carrier and thus achieve a material bond. Numerous factors must be taken into account here, which are first determined and then qualified. Accordingly, weldable strain gauges are to be integrated in components during PBF-LB/M in components consisting of the nickel-chromium alloy by means of laser welding with the existing laser-scanner system.

Within this study the possibility of integrating weld-on strain gages during PBF-LB/M is to be explored. In addition to the strain gage and the cavity design, particular attention will be paid to the weld seam design and the actual welding process. For this, the necessary parameters for welding the strain gauge are first defined and then qualified in several tests. This is to ensure that the strain gage has a strength bond to the substrate material. In the following, the determined process parameters for the strain gauge connection are also applied during PBF-LB/M and a strain gauge is integrated into a carrier component. Subsequently, a vibration test method is carried out in which the forced frequencies of the integrated strain gauge are recorded and converted into measurement data in order to investigate the bonding connection of the strain gauge. In the outlook, the possibilities of automated sensor integration are described.

Materials and Methods
Powder Material for PBF-LB/M

In this research, nickel-chromium powder (NickelAlloy IN718) provided by EOS GmbH [11] was processed by an AconityONE system with variable laser power and scan speed. For the manufacturing of the components the process parameters were adapted for sufficient material density. Therefore the layer thickness (30 µm), a nominal focused spot size (80µm), hatch distance (100 µm) and rotation angle 67° of scan strategy (meander) is set to a constant value. Thus results in material density of about 99.85 ± 0.05 % for a laser power of 300 W and a scan speed of 700 mm/s of the manufactured components were achieved. Process gas environment is formed by argon at a constant build temperature (no base plate heating). The powder was recycled through sieving during the several build jobs to ensure uniformity using a sieve with 68 µm mesh size.

Weld Seam Shape

With regard to the sensor connection by means of laser welding with the laser-scanner system, special care must be taken to ensure that the sensor component is fully connected and thus sufficient measurement accuracy is guaranteed. Consequently, an inadequate strain gauge connection can result in corresponding measurement deviations. For the used preparation software (Autodesk Netfabb) there is no possibility to create single weld lines during the PBF-LB/M process. Therefore, the required weld seams are realized by a contour exposure as shown in Fig. 1. This results in a weld seam length as well as a weld seam width which can be changed subsequently and thus define the weld seam dimensions.

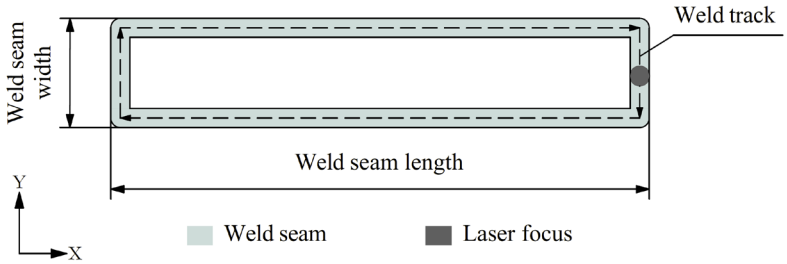

Fig. 1 Schematic representation of a weld seam

Weld Seam Analysis (Feasibility Study)

The aim of this research is to investigate the effect of process parameters such as laser power and scan speed on the melt-pool expansion of solid components during the PBF-LB/M process. Therefore, the process parameters can be used for the subsequent investigation of the metal carrier welding and ensure a firmly bonding and low thermal impact on the sensor component.

Process Parameters

For this procedure, the process parameters laser power, scan rate and focus shift were considered because these three have a decisive influence on the expansion of the melt-pool during PBF-LB/M [12]. In preliminary investigations the influence of laser power and scan speed on the material density and therefore the melt-pool expansion during PBF-LB/M were considered. This means that the largest melt pool expansion can be expected with increasing laser power at reduced scan speed.

Focus shift can be described as a distance between the build plate with a coated layer of powder and the focus plane of the laser beam [13]. The system is typically calibrated so the laser focal plane coincides with the zero-position (Fig. 2). In a PBF-LB/M system the laser focus shift measures how far the build plate is moved above (negative shift) or below (positive shift) the zero-position of the build chamber. Defocusing the laser via focus shift occurs with no changes to the laser optics, so it results in the same linear energy density but a larger spot size, and therefore has the effect of changing the area and volumetric power density.

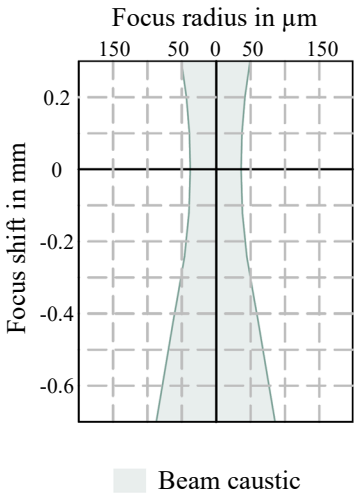

Fig. 2 Principle representation of the focus shift at zero-position

Test Specimen

The test specimen shown in Fig. 3 were manufactured using an AconityONE system with the defined process parameters for a material density of 99.85 % (±0.05 %). Then the loose metal powder around the manufactured specimen is removed from the surfaces within the PBF-LB/M machine.

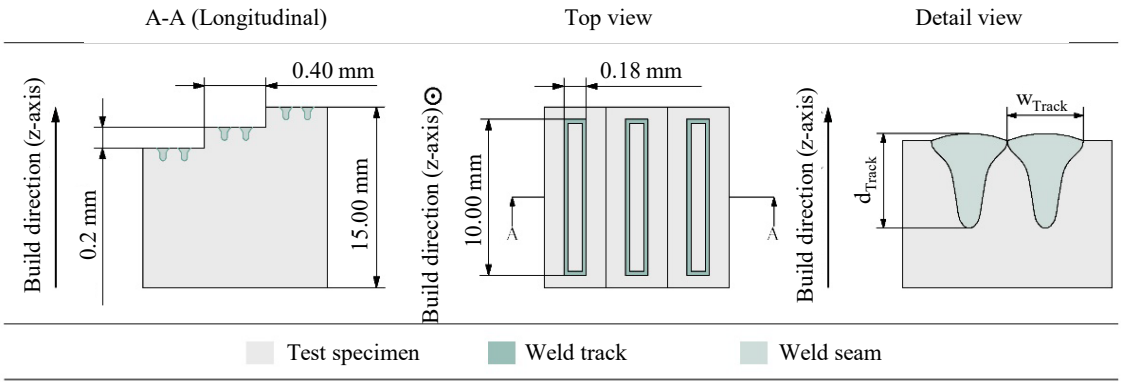

Fig. 3 Test specimen for the weld seam analysis with depth of the welding track d_{Track} and width w_{Track}

Here it is ensured that the test specimen surfaces do not contain any metal powder that can influence the expansion of the melt-pool. Subsequently, the PBF-LB/M system is again flooded with the process gas (argon) and the focus of the laser scanner system is focused on the lowest test specimen surface (lowest step), whereby the weld seams are applied with the corresponding laser powers and scanning speeds. The "steps" of the test specimens shown in Fig. 3 allow that the focus shift of the laser scanner system does not have to be changed for the weld seam application. Then the substrate plate can be removed and the weld seams applied to the test specimens can be examined.

Metal carrier welding
Process parameters

For the metal carrier welding the process parameters of the previous investigation were used. Therefore the laser power and scan speed were used to regulate the melt-pool expansion and thereby the thermal impact on the metal carrier. However further process parameters were defined to ensure a firmly bonding of the metal carrier on the component surface. In previous research it could be found out that the weld seam arrangement has a significant influence on the metal carrier connection using a laser-scanner system [14].

Test Specimen

For the metal carrier connection test specimens were designed, which have a cavity construction in which the metal carrier can be inserted. The exact dimensions are shown in Fig. 3. The test specimens were manufactured using an AconityONE and SLM 125 system with the defined process parameters for solid material components and then the surrounding metal powder was removed from the test specimens within the PBF-LB/M system. Afterwards the metal carriers are manually deposited on the cleaned cavity surfaces and the laser beam melting system was flooded again with the process gas, whereby the welds with the defined process parameters were applied in the transition area of the cavity surface and the metal carrier. The substrate plate was then removed and the weld seams applied to the test specimens were examined.

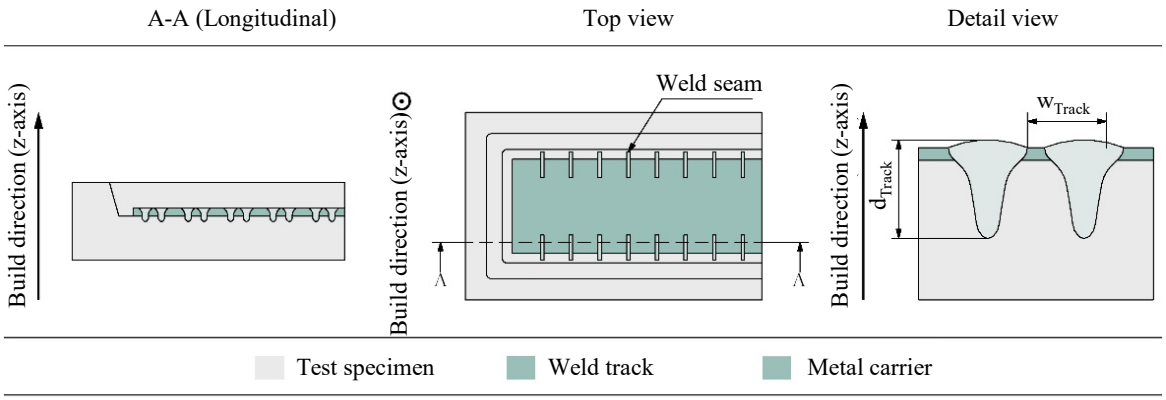

Fig. 4 Test specimen for the metal carrier welding

Metallographic methods

In this research, the specimens were prepared using standard metallographic methods. For this purpose, the specimens are cut to prepare sections as shown in Fig. 3 and Fig. 4 (see A-A and Detail view). Then the resulting relevant specimen segments were embedded. Afterwards the specimens were grounded and polished. For contrast generation, the resulting specimen sections must be etched. For this purpose, the etchant "Adler-Etching" (Etching time = 50 seconds) was used, which is mainly used for weld seam inspection of nickel-chromium alloys. Subsequently, light microscopy was performed with different magnifications, which allowed the weld seams and melt-pool expansions to be analyzed.

Results and Discussion
Weld seam analysis

For the weld seam analysis in addition to the laser power and scan speed the focus shift was also considered. The process parameter combination of laser power and scan speed can be described by the linear energy. Therefore both the laser power and scan speed were adjusted so that defined linear energies were obtained, cf. Table 1.

Table 1 Process parameters for weld seam analysis

Test combinations	Laser power in W	Scan speed in mm/s	Linear energy in J/mm
1.1	100	200	0.50
1.2	150	200	0.75
1.3	200	200	1.00
1.4	250	200	1.25
1.5	300	200	1.50
2.1	300	600	0.50
2.2	300	400	0.75
2.3	300	300	1.00
2.4	300	240	1.25
2.5	300	200	1.50

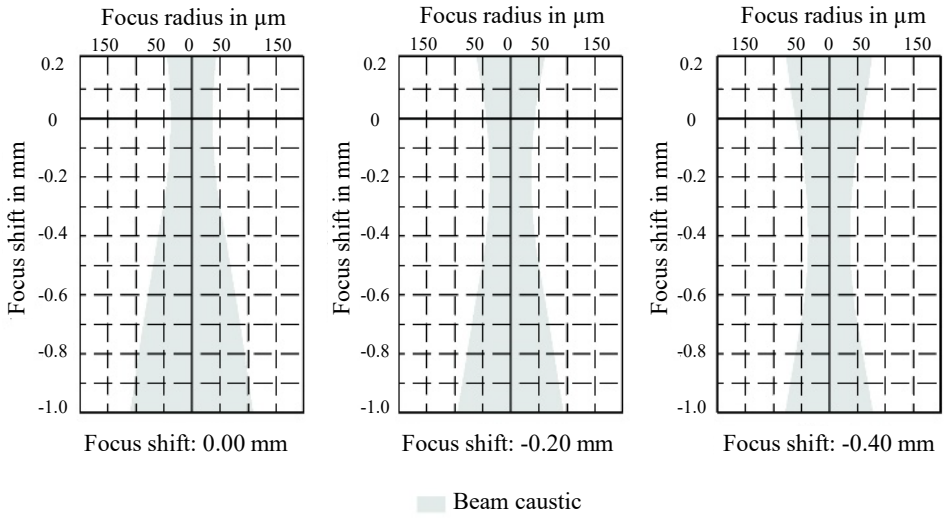

For a scanning speed of 200 mm/s (const.), the individual laser powers were changed in such a way that the individual linear energies 0.50 J/mm ≤ E_L ≤ 1.50 J/mm (ΔE_L = 0.25 J/mm) resulted. In addition, for a laser power of 300 W (const.), the corresponding scan speeds were also changed so that the same linear energies resulted. Thus it can be investigated to what extent both the laser power and the scanning speed influence the resulting melt pool expansion. For the weld seam inspection, the melt pool expansion of the same linear energies can also be examined under different laser powers and scanning speeds. For the weld seam investigation, the focus shift was changed in addition to the listed parameter combinations of laser power and scan speed, which according to Beyer should lead to an increased melt pool expansion [12].

Weld seam expansion

Fig. 5 initially shows that the weld track depth was not significantly influenced within a defined laser power and scanning speed. Slightly different weld track depths were due to measurement uncertainties caused by contrast differences in the light microscope images.

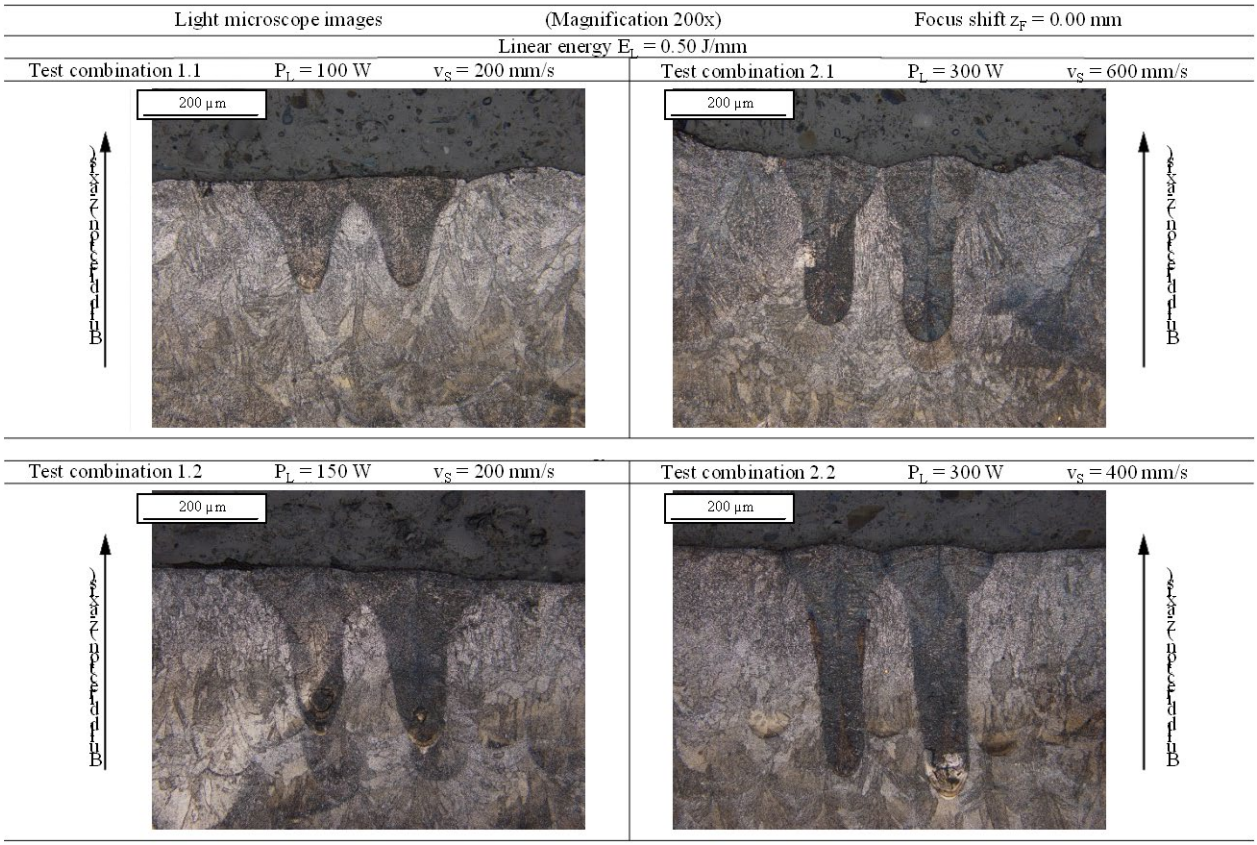

Fig. 5 Weld track depths at different laser powers

Oefele describes a so-called tolerance field for the laser scanner system, which results from the Rayleigh length of the laser beam [15]. Within this tolerance field, the weld track depth is not influenced by the focus position, since the laser beam profile hardly expands. For an increased Rayleigh length, the tolerance field of the laser beam increases at the same time, which is why the focus position should lie outside this tolerance field in order to influence the weld track depth significantly. No beam measurement documents were available at the time of this study for the

AconityONE PBF-LB/M system, which is why the Rayleigh length and the resulting tolerance field are not known. Consequently, the focus position can be considered insignificant for the weld pool expansion.

For the laser power P_L = 300 W, decreasing scan speeds and the associated increased linear energies also resulted in increased weld track depths, which differ significantly from those of the lower linear energies. This can also be observed for the scan speed v_S = 200 mm/s with increasing laser power. Accordingly, both the laser power and the scanning speed can be regarded as decisive process parameters for the melt pool expansion and the resulting weld track depth. With regard to the linear energies, it emerges that the weld track depth also increases with increasing line energy. It should be noted that different weld track depths were produced for identical linear energies under varying laser power and scan speed. Consequently, it can be concluded that there is a non-linear relationship between the energy input and the resulting weld pool expansion.

Weld seam integrity

For weld seam inspection, it is recommended to view the light microscope images of the weld seams in addition to the weld track measurement. In addition to the weld shape, this also allows the weld integrity to be assessed. Fig. 5 showed the light micrographs of the weld seams for the linear energies E_L = 0.50 J/mm and E_L = 0.75 J/mm and a focal position of z_F = 0.00 mm. Due to the low metal substrate thickness of the LS31HT strain gauge, weld track depths of 0.15 mm to 0.50 mm are considered sufficient for sensor attachment and were examined in more detail accordingly. Possible contrast differences are due to a slightly different etching time of the test specimens.

With regard to weld integrity, it can be seen that with increasing laser power and simultaneously decreasing scanning speed and resulting capillary formation within the weld track, limited material separations (microcracks) occured. According to Anik and Dorn, hot cracks can be assumed on the basis of their shape and position (Fig. 5), which occur just below the solidus temperature when the molten metal solidifies [16]. Due to the fact that the molten metal pushed out in front of the crystallization front forms isolated micro segregations and thus has a lower solidus temperature than the already solidified grains, the molten metal can no longer sufficiently compensate for the shrinkage that occurs. If the molten metal no longer flows sufficiently and the deformation capacity is exceeded, microcracks will form within the weld track. According to Anik and Dorn, nickel-chromium alloys have an increased tendency to hot cracking during the welding process. Consequently, the microsegregations of the molten metal should be reduced, which can ensure weld integrity. As a result of the lowest possible temperature gradients during the welding process through suitable process parameters (laser power and scanning speed), the microsegregations and thus the microcracks can be avoided. In addition, the shrinkage hindrance can be kept as low as possible by a suitable welding sequence, which also avoids the microsegregations.

Ultimately, it can be determined that different weld track depths result from different laser powers and scanning speeds and can accordingly be regarded as decisive for the melt pool expansion. Due to the fact that the sensor component needs not be damaged and the strain gauge LS31HT has a low metal substrate thickness, the welds resulting from the laser powers P_L = 100 W and P_L = 150 W with the corresponding scan speed v_S = 200 mm/s (test combination 1.1 and 1.2) are considered sufficient for the subsequent sensor connection. In addition, temperature gradients can thus be kept

low and weld integrity can be ensured. For the focal position, it emerges that focal positions -0.40 mm ≤ z_F ≤ 0.00 mm do not significantly influence the generated weld shape and thus focal position z_F = 0.00 mm is specified for the sensor connection.

Metal carrier connection
Preliminary test

For the preliminary test, the laser powers P_L = 100 W and P_L = 150 W already determined in the previous weld inspection were used with an associated scan speed v_S = 200 mm/s. The welding track depths thus achieved are considered sufficient to melt both the metal platelet and the underlying metal surface and to form a coherent metal melt. With the relatively low laser powers and the associated lower temperature gradients, the weld integrity can also be ensured. With regard to the weld seam investigations, it emerged that the focal position did not demonstrably influence the melt pool expansion, as a result of which a focal position z_F = 0.00 mm was provided for the metal platelet bond. Following the VDI/VDE Guideline 2635-2 [17,18] and the manufacturer's data sheet of the LS31HT strain gauge, various weld seam arrangements were defined for the laser-scanner system. Accordingly, both weld seam arrangement I and weld seam arrangement II were investigated. Table 2 lists the resulting parameter combinations for the metal plate attachment. According to VDI/VDE Guideline 2635, the metal platelets should first be provided with two tack welds (T). This is to ensure that the metal platelets can be provisionally tack-welded to the cavity support surface and that the subsequent welds can be applied correctly. Starting from the tack welds, the subsequent welds were applied according to Table 2 with the intended weld numbering on both the metal platelet and the cavity support surface, which can be expected to provide a coherent metal melt. With the Autodesk Netfabb software used, the weld width cannot be reduced arbitrarily, so the smallest possible weld width 0.18 mm was examined first. The complete weld seam dimensions are listed in Table 2 (Detail View).

Table 2 Process Parameter for Preliminary Test

Laser power in W	Scan speed in mm/s	Focus shift in mm	Weld seam width in mm
100	200	0.00	2.00
150	200	0.00	2.00

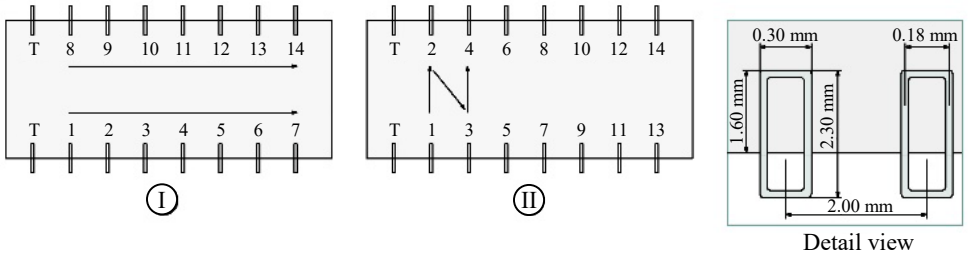

For the metal platelets, considerable material distortion can initially be demonstrated (see Fig. 6). According to Langhorst, the material distortion can be attributed to increased temperature gradients and an inhomogeneous temperature distribution within the metal platelet [19]. As a result of the finite conduction conditions of the inhomogeneously heated metal platelet, welding residual stresses result, which caused the material distortion. Especially for metal platelets, the welding-induced material distortion can be caused abruptly by material imperfections within the metal platelet and can hardly be controlled due to the unclear material situation.

Fig. 6 Weld track depths at different laser powers (width of the metal plate = 10 mm)

For the weld seam arrangement I and II, with which the laser-scanner system applied the weld seams, it can thus be determined that the successively applied weld seams cause considerable temperature gradients within the metal platelet and the associated material distortion The tack weld seams, which were intended to adhere the metal platelet to the cavity support surface, were unable to prevent the material distortion. From the metal plate images, it appears that the test combinations 1.1 and 1.2 (P_L = 100 W and v_S = 200 mm/s) were not completely welded through and thus did not result in sufficient melt pool expansion to bond the metal platelet to the cavity support surface. Consequently, a laser power P_L = 100 W with a corresponding scan speed v_S = 200 mm/s can be regarded as insufficient for the metal support bonding. For the test combinations 2.1 and 2.2, it can be seen that laser power P_L = 150 W with an associated scan speed v_S = 200 mm/s can be considered sufficient to melt both the metal platelet and the cavity support surface and form a cohesive metal melt. It should be noted here that sufficient metal platelet bonding cannot be demonstrated due to the resulting material distortion.

With regard to the VDI/VDE guideline 2635-2 and the manufacturer's data sheet of the LS31HT strain gauge, a metal carrier connection with the spot welding process is recommended, whereby the metal carrier is pressed onto the metal surface with a defined force and thus the material distortion can be compensated. For metal substrate bonding with a laser-scanner system, material distortion can only be prevented by suitable process parameters and the associated, sufficient temperature distribution. Consequently, a weld seam arrangement must be determined by which the metal substrate is heated uniformly and thus the material distortion is prevented.

Modified test

For metal platelet bonding, the laser powers P_L = 100 W and P_L = 150 W, which have already been investigated in detail, were used with the associated scan speed v_S = 200 mm/s. This means that the process parameter combinations to be investigated can be kept low. An adapted weld seam arrangement was determined for the metal substrate connection, through which the metal plate is heated as uniformly as possible and material distortion is thus prevented. Previous research has already shown that, in addition to laser power and scanning speed, multiple weld seam exposure can be regarded as an elementary process parameter [14]. Due to the fact that the metal platelets could not be completely welded with a laser power P_L = 100 W and the corresponding scan speed v_S = 200 mm/s, the metal platelets were accordingly also exposed several times. Consequently, different weld exposures result for the applied weld seam arrangement III, IV and V, which are listed in Table 3. Due to the droplet formation of the applied welds, the weld width was additionally defined as a process parameter for the metal platelet bond. In addition to the weld seam width 0.18 mm already investigated, the weld seam width 0.36 mm was therefore used. Consequently, the aim was to ensure that the adjacent weld tracks do not influence each other and that the drops of the welds can thus be avoided. Table 3 lists the modified process parameters for the metal platelet attachment.

Table 3 Process Parameter for Modified Test

Laser power in W	Scan speed in mm/s	Focus shift in mm	Weld seam width in mm
100	200	0.00	2.00
150	200	0.00	2.00
100	200	0.00	2.00
150	200	0.00	2.00

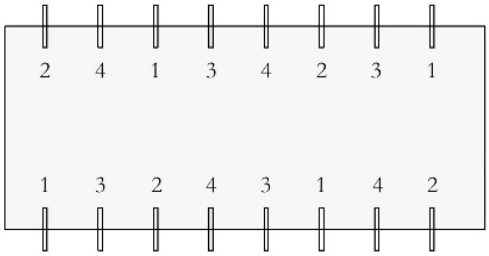

III	1 - 1 - 1 - 1 → 2 - 2 - 2 - 2 → 3 - 3 - 3 - 3 → 4 - 4 - 4 - 4	(1x Exposure)
IV	1 - 1 - 1 - 1 → 2 - 2 - 2 - 2 → 3 - 3 - 3 - 3 → 4 - 4 - 4 - 4	(3x Exposure)
V	1 - 1 - 1 - 1 (3x Exposure) → 2 - 2 - 2 - 2 (3x Exposure) → 3 - 3 - 3 - 3 (3x Exposure) → 4 - 4 - 4 - 4 (3x Exposure)	

The process parameter combinations show that only individual process parameters were changed, which allows the various process parameter influences to be assessed. With regard to VDI/VDE Guideline 2635-2, the weld seams (1) are first applied by the laser scanner system. As a result, the metal platelets were already evenly bonded to the cavity surface and material distortion was reduced. Starting from the weld seams (1), the subsequent weld seams were applied according to Table 3 with the intended weld seam numbering both on the metal platelet and on the cavity contact surface, whereby a coherent metal melt is expected. In this case, the weld seam arrangement was specifically defined to generate the largest possible spacing of the same weld seam numbering.

The metal plate bonding was performed on the SLM125 laser beam melting system, as mentioned earlier. For the modified test, the same test specimens were manufactured as before with the process

parameters mentioned for the NickelAlloy IN718 metal powder. After the metal plates have been inserted, the PBF-LB/M system was flooded again with the process gas and the weld seams applied according to the weld seam numbering with the process parameters defined in Table 3.

For the test specimen images, it can be seen that for a laser power P_L = 100 W (Test combination 1.1), there is a discernible material distortion of the metal plate. The metal plate was therefore not completely bonded to the cavity contact surface. The decisive factor here is that, due to the laser power P_L = 100 W with the associated scan speed v_S = 200 mm/s, insufficient melt pool expansion of the applied weld seams resulted. Consequently, no coherent metal melt formed, which sufficiently bonds the metal plate to the cavity support surface and counteracts material distortion. With regard to the other metal plates, which were applied with a lower power P_L = 100 W, it can be seen that these also exhibit low material distortion.

The optical micrographs show that the metal platelets were bonded to the cavity contact surface with a material bond. For a multiple weld exposure (V), it can be seen that with constant laser power P_L = 150 W, there is an increased weld track depth (compare Fig. 7). The metal platelet was heated several times by the multiple weld seam exposure, which significantly increased the molten pool expansion and resulted in sufficient metal platelet adhesion. For the single weld exposure (III), it can be seen that the melt pool expansion was lower and thus the underlying cavity contact surface melted only to a limited extent, as a result of which no sufficiently cohesive metal melt was formed.

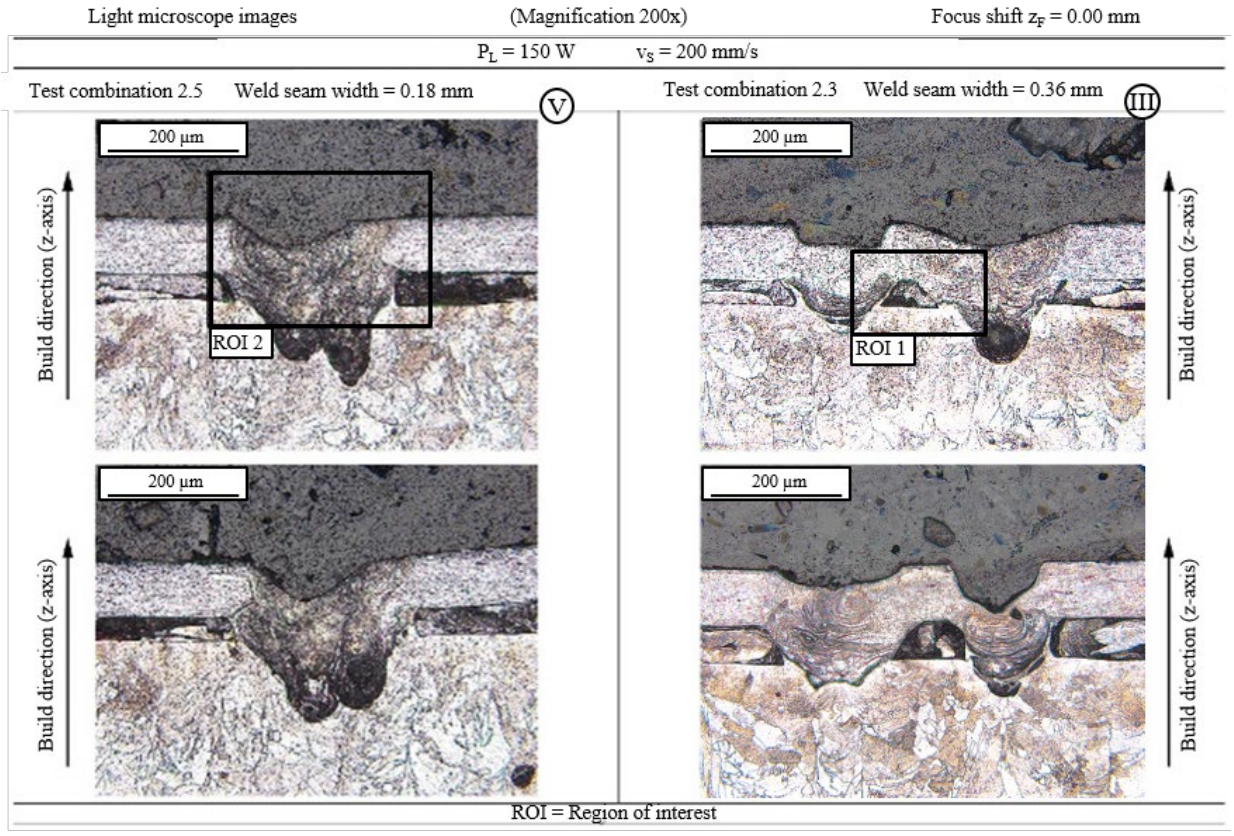

Fig. 7 Etched weld tracks between metal substrate and full base material

For the weld width, it can be seen that with an increased weld width of 0.36 mm, a significant ambient gas entrapment (ROI 1) between the metal platelet and the cavity support surface can be detected. This results from the fact that no coherent metal melt of the individual weld tracks was formed and thus individual metal melts lying next to each other were formed. For a smaller weld width of 0.18 mm, no significant flaws are discernible because the adjacent molten metal traces formed a coherent metal melt, which also melted the cavity contact surface and thus ensured an expedient metal substrate connection.

From the optical micrographs (ROI 2), it can be seen that the metal melt produced in the weld center (test combination 2.3 and 2.5) sinks. This results from the temperature gradients in the molten metal and the associated shear stresses, which led to an asymmetrical molten pool movement (Marangoni convection). Consequently, pressure gradients resulted within the molten metal, which were due to the fact that the molten metal was slowed down at the melting edge. This resulted in a pressure drop at the weld center and a pressure increase at the melt edge. As a result, the molten metal was conveyed to the melting edge and the molten metal in the weld center sinks. According to Beyer, this lowering of the molten pool describes a budding capillary formation. On the basis of the optical micrographs, the vortex-like molten pool flow caused by the Marangoni effect is evident.

In summary, the process parameters investigated (laser power P_L = 150 W and scan speed v_S = 200 mm/s) with weld exposure V and a weld width of 0.18 mm can be considered suitable for metal substrate attachment of the weldable strain gauge (compare Fig. 8).

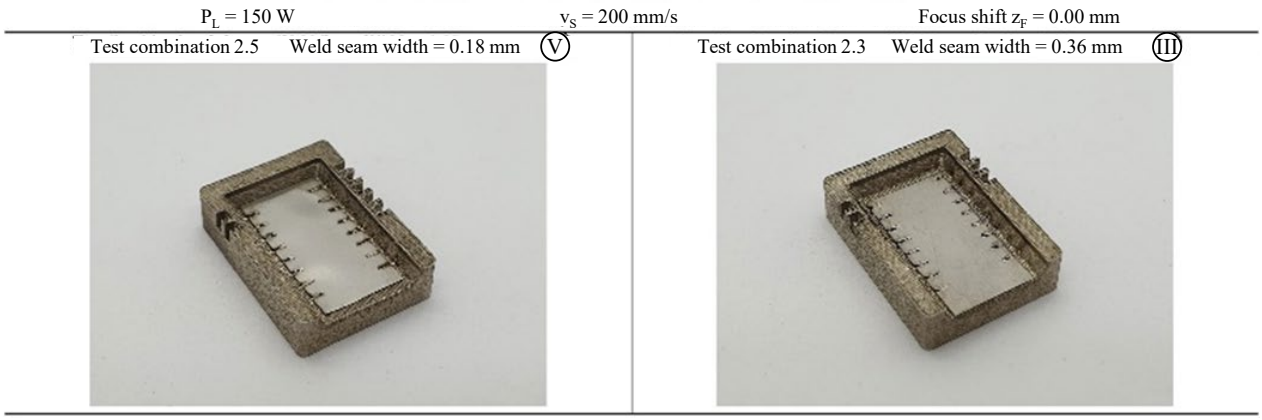

Fig. 8 Macroscopic view on the metal plates bonded to the full material IN718 component (width of the metal plate = 10 mm)

Implementation and validation

In the following, the elaborated process parameters for the sensor implementation of the strain gauge LS31HT during the PBF-LB/M process were tested in a relevant testing environment.

Gas flow measurement component

A gas flow probe (in the following called “probe rake” provided by Vectoflow GmbH was used and produced for the sensor implementation. The said components are usually manufactured by

the company Vectoflow using PBF-LB/M to measure locally occurring gas flows in a streaming field. Due to the surrounding flows, vibrations can also occur on the measurement system, which cannot be detected so far. However, vibration data is an important parameter for the design of the measurement system but also for the even more detailed testing and analysis of flow fields. The following Fig. 9 shows the probe rake manufactured out of IN718 on the SLM125 system from Vectoflow GmbH, with an integrated weldable strain gauge (WSG) using the final parameter constellation (laser power P_L = 150 W, scan speed v_S = 200 mm/s, weld exposure V, weld width 0.18 mm) for the connection of the metal plate, where the measuring grid of the strain gauge was positioned. For WSG implementation, the cavity was adapted according to the defined cavity layout for the LS31HT strain gauge. The cavity alignment in the X-Y plane resulted from the individual probe rake contour and the associated limited probe rake volume (see Fig. 9). Due to the fact that the sensor component requires a cable connection, a cable duct (X-Y plane) was provided, through which the measuring cables of the sensor component are guided out of the probe rake via the carrier plate.

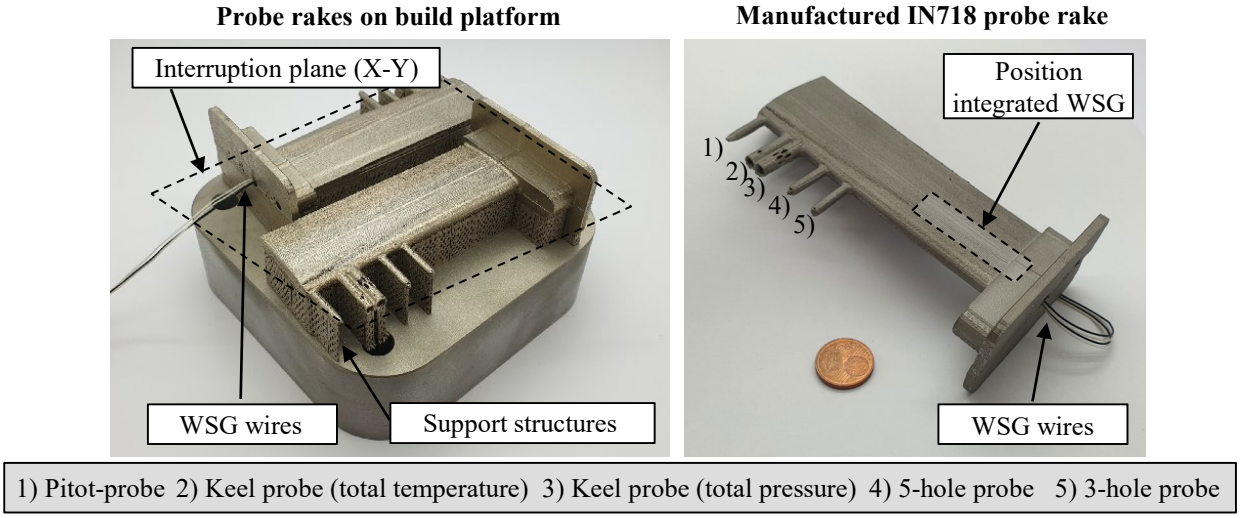

Fig. 9 Additive manufacturing of probe rakes of Vectoflow GmbH with integrated WSGs to determine occurring vibrations and forces.

Measurement data evaluation

To evaluate the proper operation of the flow rake, a test of the system for vibration detection by externally applied vibration using MIL STD 810 H was investigated. The test setup was as shown in Fig. 10, using an MX840B amplifier with a quarter-bridge circuit (350 ohm) at a sampling frequency of 1,200 Hz. A defined frequency of 350 Hz was applied to the flow rake in accordance with MIL STD 810 H via a turbine vibrator. The flow rake was then subjected to a test with a defined frequency of 350 Hz. The correctness of the vibration behavior was ensured by an externally applied Fibre Bragg Grating (FBG) sensor. In this state, the vibrations detected by the

strain gauge (WSG) were evaluated and compared with those of the FBG. Fig. 10 shows that the power maxima occured equally at 350 Hz. This confirms the correct operation of the concept.

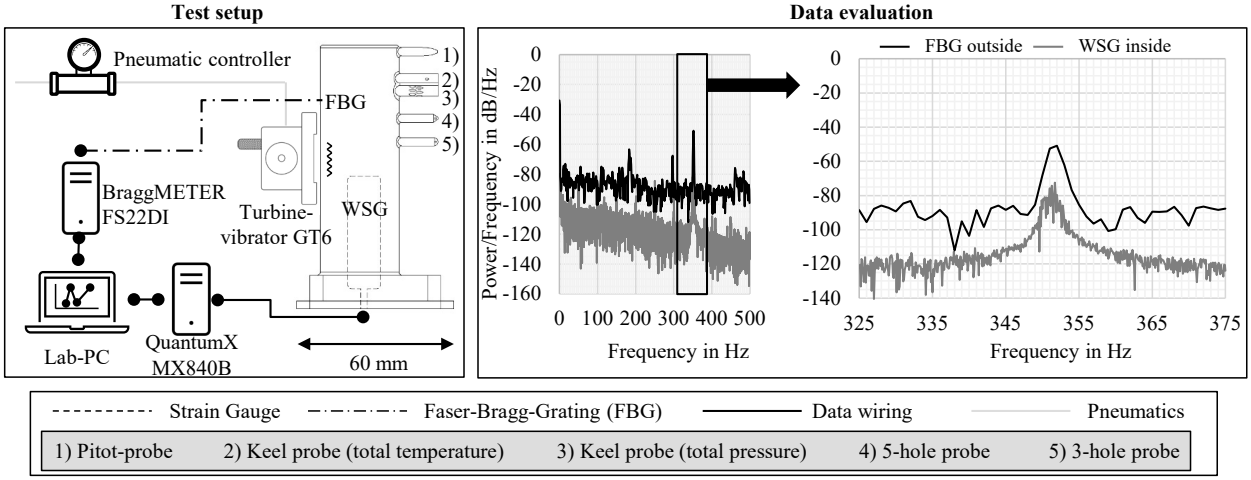

Fig. 10 Test setup for determining the correct vibration and spectral power densities of the FBG sensor and the strain gauge integrated in the flow rake in the test setup under an applied vibration of 350 Hz.

Summary and Outlook

In this work, a concept was developed with which the strain gauge LS31HT can be inserted into a component made of the metal powder Nickelalloy IN718 during the PBF-LB/M and can be attached to it. It was demonstrated that the design of the weld seams has a major influence on the material bondability of the strain gauge lamina to the rake. After successfully finding a suitable parameter combination, the configuration was used to fabricate a probe rake from Vectoflow. It was then successfully demonstrated that the integrated sensor is capable of detecting relevant vibrations.

The investigated manual sensor integration is associated with high costs, since both the personnel and the machine time must be taken into consideration for this. Furthermore, the achievable accuracy of the integration process depends on the human operator and is therefore not completely reproducible. These disadvantages can be avoided by an automated sensor integration. For this purpose, the already existing cartesian kinematic system (x-y-z-direction) described in [20] should be used for both cavity cleaning and subsequent sensor placement. The kinematic system currently being tested, which can be integrated in the AconityONE PBF-LB/M system, can pick up and place the sensors by means of a vacuum gripper. For this, the cavity must be able to be approached by the kinematic system and accordingly have an opening at the top. The kinematic system, currently under development, has a sufficient placement accuracy for the sensor component. These criteria for cavity design are met by the cavity already described, as are the criteria for sensor placement accuracy by the kinematic system. With an automated sensor integration by a kinematic system, the integration time can be reduced to a minimum and the process temperatures as well as the protective gas atmosphere can be kept at a constant level. With the use of automated sensor integration, the problems associated with the conventional method can be avoided and reproducible sensor integration can be ensured.

References

[1] C. Caviezel, R. Grünwald, S. Ehrenberg-Silies, S. Kind, T. Jetzke, M. Bovenschulte, Aditive Fertigungsverfahren (3D-Druck): Innovationsanalyse, 2017.

[2] Wohlers Associates, Wohlers Report 2020: 3D Printing and Additive Manufacturing Global State of the Industry, Fort Collins, Colorado, 2020.

[3] R. Jiang, R. Kleer, F.T. Piller, Predicting the future of additive manufacturing: A Delphi study on economic and societal implications of 3D printing for 2030, Technological Forecasting and Social Change 117 (2017) 84–97. https://doi.org/10.1016/j.techfore.2017.01.006.

[4] J. Gausemeier, Thinking ahead the Future of Additive Manufacturing - Future Applications, Paderborn, 2012.

[5] P. Harris, Reutzel, E., Earthman, J., A. Hess, Reliability Centered Additive Manufacturing Computational Design Framework, 2018.

[6] M. Binder, V. Stapff, A. Heinig, A. Schmitt, C. Seidel, G. Reinhart, Additive manufacturing of a passive, sensor-monitored 16MnCr5 steel gear incorporating a wireless signal transmission system, Lugano, 2022.

[7] M. Binder, M. Illgner, C. Anstaett, P. Kindermann, L. Kirchbichler, C. Seidel, Automated Manufacturing of Sensor-Monitored Parts, Laser Technik Journal. https://doi.org/10.1002/latj.201800015.

[8] M. Binder, C. Dirnhofer, P. Kindermann, M. Horn, M. Schmitt, C. Anstaett, G. Schlick, C. Seidel, Gunther Reinhart, Procedure and Validation of the Implementation of Automated Sensor Integration Kinematics in an LPBF System, Chicago, 2020.

[9] P. Stoll, Functionality integration in powder bed based additive manufacturing processes, 2020.

[10] DIN EN ISO/ASTM 52900:2018, Additive Manufacturing - General principles - Terminology, Beuth Verlag GmbH 52900:2018, 2018.

[11] EOS GmbH Electro Optical Systems, EOS NickelAlloy IN718 Materialdatenkennblatt, Material data sheet, 2014.

[12] E. Beyer, Schweißen mit Laser: Grundlagen, Springer, Berlin, 1995.

[13] G.E. Bean, D.B. Witkin, T.D. McLouth, R.J. Zaldivar, Process gas influence on microstructure and mechanical behavior of Inconel 718 fabricated via selective laser melting (2020).

[14] M. Binder, M. Fischer, S. Dietrich, C. Seidel, G. Reinhart, Integration of Strain Gauges in Components Manufactured by Laser-Based Powder Bed Fusion (2020).

[15] F. Oefele, Remote-Laserstrahlschweißen mit brillanten Laserstrahlquellen. Zugl.: München, Techn. Univ., Diss., 2012, Utz, München, 2013.

[16] S. Anik, L. Dorn, Schweißeignung metallischer Werkstoffe, Dt. Verl. für Schweißtechnik DVS, Düsseldorf, 1995.

[17] VDI Verein Deutscher Ingenieure e.V., Experimental structural analysis: Recommendation on the implementation of strain measurements at high temperatures 17.040.30, 2019, accessed 14 December 2020.

[18] Hottinger Baldwin Messtechnik GmbH, Dehnungsmessstreifen LI66-10/350, 2018, https://www.hbm.com/fileadmin/mediapool/hbmdoc/technical/b2156.pdf, accessed 24 April 2018.

[19] Mirko Langhorst, Beherrschung von Schweißverzug und Schweißeigenspannungen. Dissertation, München, 2015.

[20] M. Binder, C. Dirnhofer, P. Kindermann, M. Horn, M. Schmitt, C. Anstaett, G. Schlick, C. Seidel, G. Reinhart, Procedure and Validation of the Implementation of Automated Sensor Integration Kinematics in an LPBF System (2020).